

# Cardiac Magnetic Resonance 2D+T Short- and Long-axis Segmentation via Spatio-temporal SAM Adaptation

Zhenhong Chen<sup>\*,a</sup>, Sekeun Kim<sup>\*,a</sup>, Hui Ren<sup>a</sup>, Quanzheng Li<sup>a</sup>, Xiang Li<sup>a</sup>

*<sup>a</sup>Center of Advanced Medical Computing and Analysis, Massachusetts General Hospital and  
Harvard Medical School, Boston, MA, 02114, USA  
xli60@mgh.harvard.edu*

**Abstract.** Accurate 2D+T myocardium segmentation in cine cardiac magnetic resonance (CMR) scans is essential to analyze LV motion throughout the cardiac cycle comprehensively. The Segment Anything Model (SAM), known for its accurate segmentation and zero-shot generalization, has not yet been tailored for CMR 2D+T segmentation. We therefore introduce CMR2D+T-SAM, a novel approach to adapt SAM for CMR 2D+T segmentation using spatio-temporal adaptation. This approach also incorporates a U-Net framework for multi-scale feature extraction, as well as text prompts for accurate segmentation on both short-axis (SAX) and long-axis (LAX) views using a single model. CMR2D+T-SAM outperforms existing deep learning methods on the STACOM2011 dataset, achieving a myocardium Dice score of 0.885 and a Hausdorff distance (HD) of 2.900 pixels. It also demonstrates superior zero-shot generalization on the ACDC dataset with a Dice score of 0.840 and a HD of 4.076 pixels.

**Keywords:** Cardiac magnetic resonance, Image segmentation, Foundational Model

## 1 Introduction

While the left ventricular (LV) ejection fraction (EF) derived from two cardiac phases, end-diastole (ED) and end-systole (ES), remains the major clinical parameter for diagnosis and prognosis in heart failure[1], it falls short in certain heart diseases such as dyssynchrony and diastolic heart failure which demand a more thorough temporal analysis that extends beyond the ED and ES phases. Therefore, 2D+T segmentation offering a comprehensive view of LV motion throughout the entire cardiac cycle is crucial. Specifically, 2D+T segmentation in cine cardiac magnetic resonance (CMR) involves the delineation of myocardium for every cardiac phase within each slice. It can also be considered as medical video segmentation.

**Existing deep learning (DL) approaches:** DL approaches for 2D+T CMR segmentation necessitates understanding of the spatial information as well as the temporal dynamics and consistency across all cardiac phases. Existing methods primarily fall into two strategies: (1) 3D U-Net methods that treat temporal sequences as depth dimension [2], and (2) 2D U-Net with a recurrent layer (e.g., Conv-LSTM) to capture temporal

\* Co-first authors.

dependences between phases[3], [4], [5]. Researchers have also explored the application of optical flow for temporal coherence[6], [7] and combined motion estimation with segmentation to overcome the limited availability of comprehensive ground truth labels[8]. Regularization based on known cardiac behaviors, such as smooth temporal motion, decreasing volume size in the systole and the same area variation tendency between endo- and epicardium, is also applied[9], [10]. Although several work [10], [11] have tackled 3D+T segmentation, it may be constrained by several artifacts[12] of the volumetric CMR images, including large slice thickness, lack of slice coverage and inter-slice misalignment due to cardiac motion, which all compromise the fidelity of 2D slice stacks as representations of the actual 3D volume. Our focus on 2D+T segmentation helps to sidestep these complications.

**Our SAM adaptation:** Segment Anything Model (SAM)[13] is a visual foundation model trained on one-billion-image dataset, renowned for its segmentation accuracy and zero-shot generalization. However, direct application of SAM to medical imaging, even with prompt guidance, led to suboptimal performance[14], [15], [16]. To improve compatibility, recent efforts mainly focus on parameter-efficient transfer learning techniques such as adding Adapter modules. Furthermore, adapting the 2D SAM model for 3D medical images has involved unique adapter modifications such as adding 3D convolution [17], [18] or using parallel branches for spatial and depth dimensions[19]. Medical video (i.e., 2D+T) adds a temporal dimension to 2D images, providing critical time-related context. Recently, Kim et al.[16] attempted to adapt SAM to 2D+T echocardiography segmentation using TimeSformer[20] (space-time self-attention) as the “spatio-temporal adapter”. Inspired by this work, we have developed an innovative 2D+T CMR myocardium segmentation model via spatio-temporal SAM adaptation, called CMR2D+T-SAM, with four key technical components. The first three are: (1) the vision transformer (ViT) blocks from the SAM model to exploit pre-trained SAM weights, (2) a spatio-temporal adapter powered by TimeSformer to adapt SAM for 2D+T data, and (3) a U-Net framework serving as the image encoder and mask decoder to ensure the multi-scale spatial understanding. The fourth and unique feature is the ability to handle segmentation on both short-axis (SAX) and long-axis (LAX) views using a single model, guided by textual prompts to specify input view type.

To validate our method, we first focused on SAX segmentation. The CMR2D+T-SAM-SAX model was trained on SAX images without the prompt feature. Firstly, we compared our method with existing approaches on STACOM2011 dataset[21] to illustrate its superior myocardium segmentation accuracy. We then showed superior zero-shot generalization of our method on the independent ACDC dataset[22]. Lastly, we extended the investigation on multi-types of views. We trained the model, CMR2D+T-SAM-Multi with the text prompt feature on both SAX and LAX views and demonstrated its high performance on both types of views.

## 2 Methods

In this section, we introduce each of the 4 key components of CMR2D+T-SAM. **Fig.1** displays the overall model structure. The model input is 2D+T CMR SAX or LAX data

with dimensions  $[H, W, T]$ , where  $H$  and  $W$  denote the height and width of a slice, and  $T$  denotes the number of the cardiac phases it captures in one cardiac cycle.

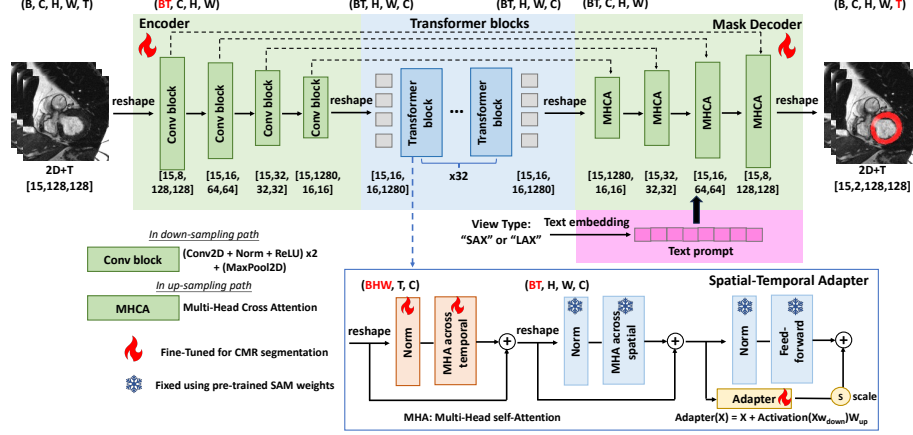


**Fig. 1.** The overall structure of CMR2D+T-SAM model. It includes (1) Refined ViT blocks with SAM weights (blue section); (2) Spatio-temporal adaptation (blue section); (3) U-Net framework as encoder and decoder (green section); (4) Text prompts to specify the view type (pink section). Components undergoing fine-tuning for CMR segmentation are denoted by a "fire" icon, whereas those retaining pre-trained SAM weights are marked with a "snowflake" icon. Data dimension transitions for each module are annotated above the respective sections, where  $B$  = batch size,  $C$  = channel number,  $H$  and  $W$  = height and width of the input, and  $T$  = the number of frames.

## 2.1 Model Main Technical Components

**Component 1 - ViT Blocks with Pre-trained SAM Weights:** The SAM initially has three main parts: an image encoder, a prompt encoder and a mask decoder, all pre-trained on a vast one-billion-image dataset. The image encoder features a series of ViT blocks, critical for SAM’s effectiveness in downstream tasks. As shown in the blue section of **Fig.1**, our CMR2D+T-SAM leverages the “vit-h” variant with 32 transformer blocks. We freeze the pre-trained SAM weights within each transformer block (marked by the “snowflake” icon in **Fig.1**), enabling our model to harness SAM’s task-agnostic segmentation and generalization capabilities.

**Component 2 - Refined ViT blocks with Spatio-temporal adaptation:** Similar as TimeSformer (the space-time self-attention model)[20], we refined the ViT blocks to have temporal attention and spatial attention sequentially applied one after the other, thus integrating spatio-temporal information. The layers in one refined ViT block is shown in **Fig.1**’s blue box. Concretely, for ViT input data  $X \in \mathbb{R}^{BT \times H \times W \times C}$ , we first reshape it into the dimension of  $(BHW \times T \times C)$  and input it into the multi-head attention (MHA) module working on temporal dimension (“T” dimension). Subsequently, we reshape the data to  $(BT \times H \times W \times C)$  and feed it into the MHA working on the spatial dimension (“H” and “W” dimension). Followed by the spatial attention, we apply an adapter and scale its output using a scaling factor (empirically  $s = 0.5$ ) to balance

the task-agnostic features and the task-specific features[23]. We fixed the spatial attention and feed-forward layer weights from the pre-trained SAM, while the other layers are trained for the task of CMR segmentation (marked by the “fire” icon in Fig.1).

**Component 3 – the U-Net framework:** Recognizing the value of multi-scale feature extraction in medical image segmentation, we leveraged a U-Net framework within CAM2D+T-SAM’s image encoder and lightweight mask decoder (green sections in Fig.1). Concretely, within SAM image decoder, we substitute the original patch embedding code with the downsampling pathway of a 2D U-Net. The 2D+T CMR input  $X \in \mathbb{R}^{B \times C \times H \times W \times T}$  is reshaped into  $\mathbb{R}^{(BT) \times C \times H \times W}$ , allowing for 2D convolutional and pooling operations on spatial dimensions to derive multi-scale features. Further, within SAM mask decoder, we replace the original mask embedding’s upsampling code with the 2D U-Net’s upsampling pathway, which includes skip connections to the downsampling pathway. Inspired by U-Net Transformer[24], each stage of the U-Net’s upsampling pathway is enhanced by incorporating a multi-head cross-attention (MHCA) module following two convolutions, which reduces noise and irrelevant elements in the skip-connected features. All U-Net layers were fine-tuned for CMR segmentation.

**Component 4 – Text prompt to specify the view type:** The existing 2D+T DL segmentation methods predominantly address SAX segmentation. However, the LAX views are also very important as it provides high-resolution data along the z-axis and critical clinical parameters such as global longitudinal strain. Therefore, our goal is to equip CAM2D+T-SAM with the capability to segment both SAX and LAX 2D+T data using a *single* model. We leverage the prompt feature of the SAM model to specify the model input’s view type (i.e., SAX or LAX). Concretely, we use the text “SAX” and “LAX” as two text prompts for SAX and LAX data respectively. The text is embedded using the pre-trained CLIP model[25] and then integrated into SAM’s mask decoder using the same way as how the sparse prompt embedding (e.g., point, box...) is integrated. The effectiveness of using prompts versus training directly on SAX and LAX data without prompts will be assessed in the Results section.

## 2.2 Implementation Details

CAM2D+T-SAM classifies myocardium and background. The model was trained using a weighted sum of binary cross-entropy and Dice loss. We employed the MADGRAD optimizer[26] with an initial learning rate of  $10^{-4}$ , which is decayed every 100 epochs. For preprocessing 2D+T data, SAX or LAX slices were center-cropped to  $[H, W] = [128, 128]$  with T sampled to 15 phases, including ED and ES. Image intensities were normalized to  $[0, 1]$  via min-max normalization method. To enhance robustness, data augmentations such as random translations, rotations, flips, noise injection, contrast and brightness alterations were applied. The model was trained and tested on a single DGX-A100 GPU (NVIDIA, CA, USA) and consumed around 20GB GPU memory.

## 2.3 Evaluation Tasks

In evaluation tasks 1 and 2, we focus on the SAX 2D+T segmentation with the CMR2D+T-SAM-SAX model, specifically trained on SAX data. In evaluation task 3, we expand our analysis to both SAX and LAX segmentation. The CMR2D+T-SAM-

LAX means the model trained only on LAX images, while CMR2D+T-SAM-Multi denotes the model trained on both SAX and LAX images. Segmentation accuracy was measured using Dice coefficient and Hausdorff distance (HD), reported as mean values.

**Task 1: Evaluate the SAX 2D+T segmentation accuracy.** In this task, we utilized the public dataset, STACOM2011[21], which includes 100 cine CMR scans from 100 patients with coronary artery diseases and prior myocardial infarction. The manual 2D+T (all cardiac phases) segmentation of myocardium were provided. The first 60 scans were used for training and the rest 40 were used for testing. We compared myocardium segmentation of our CMR2D+T-SAM-SAX model with existing DL methods including naïve 2D U-Net, 3D U-Net[2], 2D U-Net with recurrent layers[3], [4] and 3D nnUNet[27]. Uniquely, we reported the performance for basal, mid-cavity and apical slices separately to see the dependence of performance on the slice position.

**Task 2: Evaluate the zero-shot generalization capability.** Our model's zero-shot generalization was evaluated by training on the entire STACOM2011 and then testing on another independent public dataset, ACDC dataset[22], without any further training or fine-tuning. ACDC dataset comprises 150 cine CMR scans across 5 physiological classes. The evaluation was done on ED and ES phases which are only two phases with manual ground truth in ACDC dataset. Our model's zero-shot generalization performance was compared with the DL methods mentioned in Task 1.

**Task 3: Evaluate the multi-view segmentation accuracy and the effectiveness of text prompt.** We compared four model settings: (1) CMR2D+T-SAM-SAX, (2) CMR2D+T-SAM-LAX, (3) CMR2D+T-SAM-Multi without text prompt and (4) CMR2D+T-SAM-Multi with text prompt. By comparing (3) or (4) with (1) and (2), we analyzed the feasibility of using a *single* model to segment both types of views while maintaining the accuracy as view-specific models. By comparing (4) with (3), we evaluated the effectiveness of text prompt. All models were trained on the first 60 scans in STACOM2011 and tested on the rest 40 scans. STACOM2011 offers manual 2D+T segmentation for both SAX stack and multiple LAX views, and all LAX views were used into this experimental assessment.

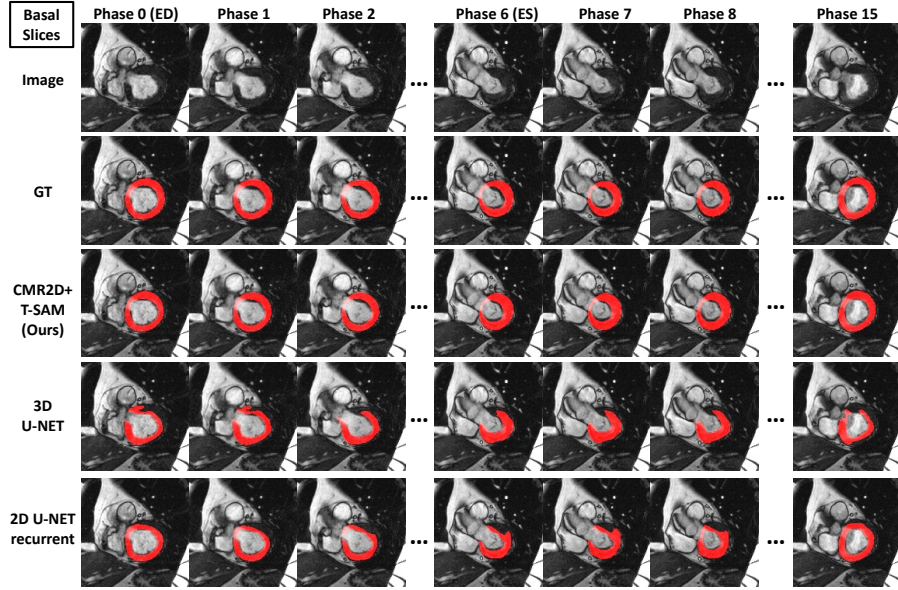
### 3 Evaluation Results

**Task 1: Table 1** shows the superior segmentation accuracy in terms of the highest Dice and the lowest HD of CMR2D+T-SAM over other existing DL methods in the STACOM dataset. Notably, segmentation accuracy was higher in the base and mid-cavity slices compared to the apical slices across all methods. Quantitatively, CMR2D+T-SAM-SAX achieved Dice = 0.885 and HD = 2.900 pixels for all slices. **Fig.2** present examples that illustrate the accuracy and phase-to-phase consistency of our model's predictions, a level of accuracy and consistency not observed in the existing methods (other methods depicted in the 4<sup>th</sup> and 5<sup>th</sup> rows of **Fig.2**).

**Task 2: Table 2** demonstrate the superior zero-shot generalization of CMR2D+T-SAM-SAX over other existing DL methods in the ACDC dataset. Again, segmentation accuracy was higher in the base and mid-cavity slices compared to the apical slices across all methods. Concretely, CMR2D+T-SAM-SAX achieved Dice = 0.840 (decrease 4.5% compared to STACOM results) and HD = 4.076 pixels for all slices. **Fig.4** present the zero-shot generalization of our model for all three slice positions.

**Table 1.** Results on STACOM Dataset. HD = Hausdorff Distance (unit = pixel).

Metric	Method	All slices	Basal slices	Mid slices	Apical slices
Dice	2D U-Net	0.810	0.828	0.825	0.760
	3D U-Net[2]	0.835	0.850	0.843	0.797
	2D recurrent U-Net[3], [4]	0.860	0.876	0.873	0.811
	nnUNet-3D[27]	0.872	0.886	0.882	0.835
	CMR2D+T-SAM-SAX (ours)	<b>0.885</b>	<b>0.895</b>	<b>0.897</b>	<b>0.847</b>
HD (pixel)	2D U-Net	7.478	7.708	7.148	7.666
	3D U-Net[2]	5.766	5.689	5.954	5.623
	2D recurrent U-Net[3], [4]	3.947	3.672	3.855	4.467
	nnUNet-3D[27]	3.811	3.961	3.610	3.955
	CMR2D+T-SAM-SAX (ours)	<b>2.900</b>	<b>2.764</b>	<b>2.743</b>	<b>3.336</b>

**Fig. 2.** STACOM SAX results on basal slices. These examples show the accuracy (compared to GT) and phase-to-phase consistency of our model's predictions.

**Table 2.** Zero-shot on ACDC Dataset.

Metric	Method	All slices	Basal slices	Mid slices	Apical slices
Dice	3D U-Net[2]	0.787	0.810	0.790	0.756
	2D recurrent U-Net[3], [4]	0.820	0.845	0.824	0.762
	nnUNet-3D[27]	0.790	0.821	0.800	0.742
	CMR2D+T-SAM-SAX (ours)	<b>0.840</b>	<b>0.872</b>	<b>0.845</b>	<b>0.793</b>
HD (pixel)	3D U-Net[2]	8.547	9.086	8.800	7.166
	2D recurrent U-Net[3], [4]	5.388	5.006	5.603	5.998
	nnUNet-3D[27]	6.409	6.663	6.114	6.632
	CMR2D+T-SAM-SAX (ours)	<b>4.076</b>	<b>3.740</b>	<b>4.048</b>	<b>4.434</b>

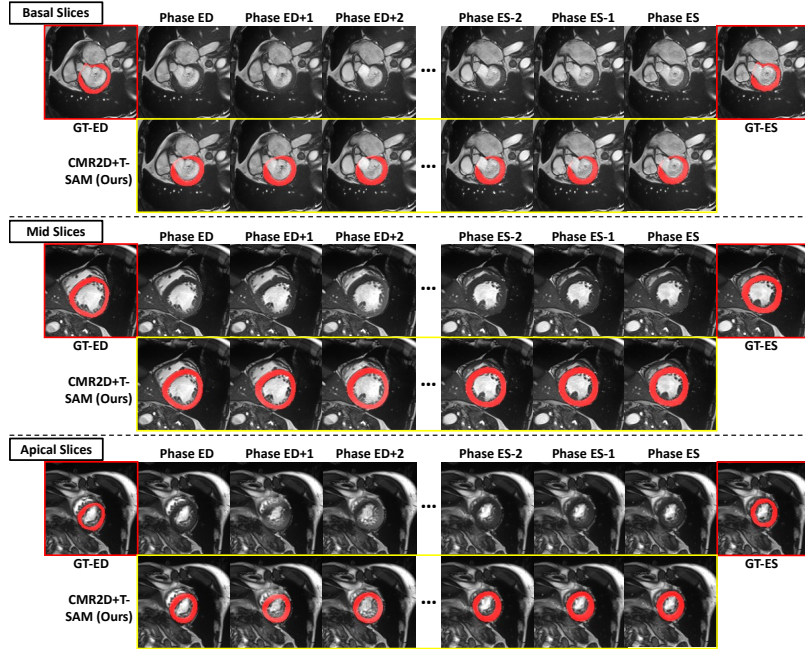


**Fig. 3.** Zero-shot generalization on ACDC dataset. Our model shows accuracy on labeled phases (ED and ES) and consistency across unlabeled phases (between ED and ES) in all three slice positions. Particularly in basal slices, our model delineates the left ventricular outflow tract (LVOT) boundary in a manner that mirrors the manual annotations of the STACOM dataset, indicating effective learning by the model.

**Task 3:** Table 3 presents the SAX and LAX performance using four different model settings mentioned in section 2.6. A comparison between (3) and (4) against (1) or (2)

indicates that a single model trained on both views can match or exceed the accuracy of view-specific models trained on SAX or LAX alone. Note that the LAX segmentation accuracy shows a marginal improvement in (3) and (4), likely benefiting from the additional training data provided by the SAX dataset. Furthermore, the direct comparison of models (4) versus (3) suggests that the incorporation of text prompts yields a slight enhancement for both SAX and LAX views. **Fig.4** presents the results of (4) CMR2D+T-SAM-Multi with prompt in two-chamber, three-chamber and four-chamber LAX views. For a comprehensive breakdown of Dice and HD across all SAX slice positions, please refer to the **supplemental material Table 1**.

**Table 3.** Multi-view segmentation accuracy on STACOM dataset.

	SAX		LAX	
	Dice	HD (pixel)	Dice	HD (pixel)
(1) CMR2D+T-SAM-SAX	0.885	2.900	/	/
(2) CMR2D+T-SAM-LAX	/	/	0.831	6.371
(3) CMR2D+T-SAM-Multi w/o prompt	0.876	3.030	0.837	6.264
(4) CMR2D+T-SAM-Multi w/ prompt	0.881	3.028	0.840	5.733

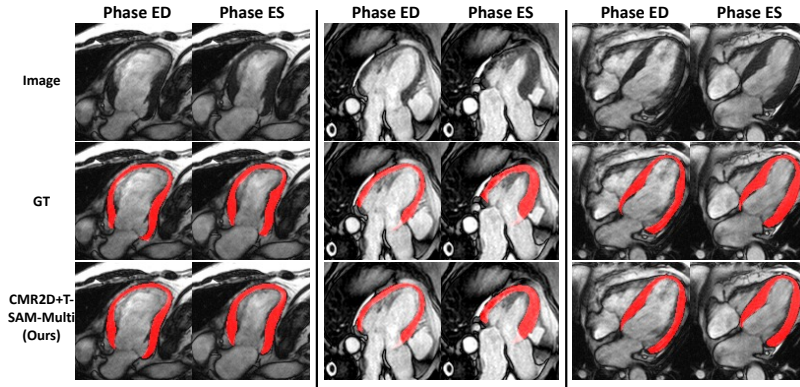


**Fig. 4.** LAX segmentation of CMR2D+T-SAM-Multi with text prompt. From left to right are two-chamber, three-chamber, and four-chamber views segmentation in the STACOM dataset.

## 4 Conclusions

In this study, we propose CMR2D+T-SAM which employs ViT blocks with pre-trained SAM weights and spatio-temporal adaptation, structured within a U-Net framework. This model delivers accurate and consistent 2D+T myocardium segmentation throughout all cardiac phases within a single cardiac cycle in cine CMR scans. Incorporating text prompts, our model adeptly manages segmentation across both SAX and LAX views, laying groundwork for future adaptability to diverse inputs. Future work involves validation using multi-center clinical CMR datasets and the derivation of clinical parameters from the segmentation results.



## References

- [1] G. Savarese, D. Stolfo, G. Sinagra, and L. H. Lund, “Heart failure with mid-range or mildly reduced ejection fraction,” *Nat Rev Cardiol*, vol. 19, no. 2, Art. no. 2, Feb. 2022, doi: 10.1038/s41569-021-00605-5.
- [2] J. Patravali, S. Jain, and S. Chilamkurthy, “2D-3D Fully Convolutional Neural Networks for Cardiac MR Segmentation.” arXiv, Jul. 31, 2017. doi: 10.48550/arXiv.1707.09813.
- [3] N. Savioli, M. S. Vieira, P. Lamata, and G. Montana, “Automated segmentation on the entire cardiac cycle using a deep learning work-flow.” arXiv, Aug. 31, 2018. doi: 10.48550/arXiv.1809.01015.
- [4] “Cardiac-DeepIED: Automatic Pixel-Level Deep Segmentation for Cardiac Bi-Ventricle Using Improved End-to-End Encoder-Decoder Network,” *IEEE J Transl Eng Health Med*, vol. 7, p. 1900110, Feb. 2019, doi: 10.1109/JTEHM.2019.2900628.
- [5] S. Vesal, M. Gu, A. Maier, and N. Ravikumar, “Spatio-Temporal Multi-Task Learning for Cardiac MRI Left Ventricle Quantification,” *IEEE Journal of Biomedical and Health Informatics*, vol. 25, no. 7, pp. 2698–2709, Jul. 2021, doi: 10.1109/JBHI.2020.3046449.
- [6] W. Yan, Y. Wang, Z. Li, R. J. van der Geest, and Q. Tao, “Left Ventricle Segmentation via Optical-Flow-Net from Short-Axis Cine MRI: Preserving the Temporal Coherence of Cardiac Motion,” in *Medical Image Computing and Computer Assisted Intervention – MICCAI 2018*, A. F. Frangi, J. A. Schnabel, C. Davatzikos, C. Alberola-López, and G. Fichtinger, Eds., in Lecture Notes in Computer Science. Cham: Springer International Publishing, 2018, pp. 613–621. doi: 10.1007/978-3-030-00937-3\_70.
- [7] S. Queirós *et al.*, “Fast automatic myocardial segmentation in 4D cine CMR datasets,” *Medical Image Analysis*, vol. 18, no. 7, pp. 1115–1131, Oct. 2014, doi: 10.1016/j.media.2014.06.001.
- [8] C. Qin *et al.*, “Joint Learning of Motion Estimation and Segmentation for Cardiac MR Image Sequences.” arXiv, Jun. 11, 2018. doi: 10.48550/arXiv.1806.04066.
- [9] G. Luo, K. Wang, S. Cao, Q. Li, and H. Zhang, “A Temporal Area Variation Regularized Deep Learning Network for Left Ventricle Segmentation on CMR,” in *2018 Computing in Cardiology Conference (CinC)*, Sep. 2018, pp. 1–4. doi: 10.22489/CinC.2018.076.
- [10] X. Qi, Y. He, Y. Qi, Y. Kong, G. Yang, and S. Li, “STANet: Spatio-Temporal Adaptive Network and Clinical Prior Embedding Learning for 3D+T CMR Segmentation,” *IEEE J Biomed Health Inform*, vol. 28, no. 2, pp. 881–892, Feb. 2024, doi: 10.1109/JBHI.2023.3337521.
- [11] A. Myronenko *et al.*, “4D CNN for Semantic Segmentation of Cardiac Volumetric Sequences,” in *Statistical Atlases and Computational Models of the Heart. Multi-Sequence CMR Segmentation, CRT-EPiggy and LV Full Quantification Challenges*, M. Pop, M. Sermesant, O. Camara, X. Zhuang, S. Li, A. Young, T. Mansi, and A. Suinesiaputra, Eds., in Lecture Notes in Computer Science. Cham: Springer International Publishing, 2020, pp. 72–80. doi: 10.1007/978-3-030-39074-7\_8.
- [12] S. E. Petersen *et al.*, “UK Biobank’s cardiovascular magnetic resonance protocol,” *Journal of Cardiovascular Magnetic Resonance*, vol. 18, no. 1, p. 8, Feb. 2016, doi: 10.1186/s12968-016-0227-4.
- [13] A. Kirillov *et al.*, “Segment Anything.” arXiv, Apr. 05, 2023. doi: 10.48550/arXiv.2304.02643.

- [14] Y. Huang *et al.*, “Segment anything model for medical images?,” *Medical Image Analysis*, vol. 92, p. 103061, Feb. 2024, doi: 10.1016/j.media.2023.103061.
- [15] M. A. Mazurowski, H. Dong, H. Gu, J. Yang, N. Konz, and Y. Zhang, “Segment anything model for medical image analysis: An experimental study,” *Medical Image Analysis*, vol. 89, p. 102918, Oct. 2023, doi: 10.1016/j.media.2023.102918.
- [16] S. Kim *et al.*, “MediViSTA-SAM: Zero-shot Medical Video Analysis with Spatio-temporal SAM Adaptation.” arXiv, Nov. 13, 2023. Accessed: Jan. 10, 2024. [Online]. Available: <http://arxiv.org/abs/2309.13539>
- [17] J. Pan, Z. Lin, X. Zhu, J. Shao, and H. Li, “ST-Adapter: Parameter-Efficient Image-to-Video Transfer Learning.” arXiv, Oct. 13, 2022. doi: 10.48550/arXiv.2206.13559.
- [18] S. Gong *et al.*, “3DSAM-adapter: Holistic Adaptation of SAM from 2D to 3D for Promptable Medical Image Segmentation.” arXiv, Jun. 23, 2023. doi: 10.48550/arXiv.2306.13465.
- [19] J. Wu *et al.*, “Medical SAM Adapter: Adapting Segment Anything Model for Medical Image Segmentation.” arXiv, Dec. 28, 2023. doi: 10.48550/arXiv.2304.12620.
- [20] G. Bertasius, H. Wang, and L. Torresani, “Is Space-Time Attention All You Need for Video Understanding?” arXiv, Jun. 09, 2021. doi: 10.48550/arXiv.2102.05095.
- [21] A. Suinesiaputra *et al.*, “A collaborative resource to build consensus for automated left ventricular segmentation of cardiac MR images,” *Med Image Anal*, vol. 18, no. 1, pp. 50–62, Jan. 2014, doi: 10.1016/j.media.2013.09.001.
- [22] O. Bernard *et al.*, “Deep Learning Techniques for Automatic MRI Cardiac Multi-Structures Segmentation and Diagnosis: Is the Problem Solved?,” *IEEE Trans Med Imaging*, vol. 37, no. 11, pp. 2514–2525, Nov. 2018, doi: 10.1109/TMI.2018.2837502.
- [23] S. Chen *et al.*, “AdaptFormer: Adapting Vision Transformers for Scalable Visual Recognition.” arXiv, Oct. 14, 2022. doi: 10.48550/arXiv.2205.13535.
- [24] O. Petit, N. Thome, C. Rambour, and L. Soler, “U-Net Transformer: Self and Cross Attention for Medical Image Segmentation.” arXiv, Mar. 12, 2021. doi: 10.48550/arXiv.2103.06104.
- [25] A. Radford *et al.*, “Learning Transferable Visual Models From Natural Language Supervision.” arXiv, Feb. 26, 2021. doi: 10.48550/arXiv.2103.00020.
- [26] A. Defazio and S. Jelassi, “Adaptivity without Compromise: A Momentumized, Adaptive, Dual Averaged Gradient Method for Stochastic Optimization.” arXiv, Aug. 26, 2021. doi: 10.48550/arXiv.2101.11075.
- [27] F. Isensee, P. F. Jaeger, S. A. A. Kohl, J. Petersen, and K. H. Maier-Hein, “nnU-Net: a self-configuring method for deep learning-based biomedical image segmentation,” *Nat Methods*, vol. 18, no. 2, Art. no. 2, Feb. 2021, doi: 10.1038/s41592-020-01008-z.